Physica B 521 (2017) 198–203

Contents lists available at ScienceDirect

Physica B

journal homepage: www.elsevier.com/locate/physb

Temperature dependence of theoretical and experimental Debye-Waller factors, thermal expansion and XAFS of metallic Zinc

Nguyen Van Hung[a,*], Cu Sy Thang[b,f], Nguyen Ba Duc[c], Dinh Quoc Vuong[d], Tong Sy Tien[e]

[a] Department of Physics, Hanoi University of Science, 334 Nguyen Trai, Thanh Xuan, Hanoi, Vietnam
[b] Institute of Geological Sciences (IGS), Vietnam Academy of Science and Technology (VAST), 18 Hoang Quoc Viet, Cau Giay, Ha Noi, Vietnam
[c] Department of Physics, Tan Trao University, Km6, Trung Mon, Yen Son, Tuyen Quang, Vietnam
[d] Quang Ninh Education & Training Department, Nguyen Van Cu, Ha Long, Quang Ninh, Vietnam
[e] Department of Basic Sciences, University of Fire Fighting & Prevention, 243 Khuat Duy Tien, Thanh Xuan, Hanoi, Vietnam
[f] Graduate University of Science and Technology, Vietnam Academy of Science and Technology (VAST), 18 Hoang Quoc Viet, Cau Giay, Ha Noi, Vietnam

ARTICLE INFO

Keywords:
Debye-Waller factor
Cumulants
XAFS
Fourier transform magnitudes
Hcp crystals

ABSTRACT

Debye-Waller factors presented in terms of cumulant expansion up to the third order, thermal expansion coefficient, X-ray absorption fine structure (XAFS) spectra and their Fourier transform magnitudes of Zn (hcp crystal) have been calculated and measured. The results have been obtained based on the quantum statistically derived method using that the calculations and measurements are necessary only for the second cumulants from which all other XAFS parameters have been provided. The many-body effects included in the present one-dimensional model are taken into account based on the first shell near neighbor contributions to the vibration between absorber and backscaterer atoms. Morse potential is assumed to describe the single-pair atomic interaction included in the anharmonic interatomic effective potential. Numerical results for Zn are found to be in good agreement with the obtained experimental data which show evident temperature dependence of the thermodynamic properties, anharmonic effects and structural parameters of the material.

1. Introduction

X-ray Absorption Fine Structure (XAFS) has developed into a powerful technique for providing information on the local atomic structure and thermal effects of substances. The formalism for including anharmonic effects in XAFS is often based on cumulant expansion approach [1] from which the anharmonic XAFS function has resulted as

$$\chi(k) = F(k)\frac{e^{-2R/\lambda(k)}}{kR^2}\mathrm{Im}\left\{e^{i\Phi(k)}\exp\left[2ikR + \sum_n \frac{(2ik)^n}{n!}\sigma^{(n)}\right]\right\}, \quad (1)$$

where F(k) is the real atomic backscattering amplitude, k and λ are the wave number and mean free path of photoelectron, respectively, Φ is the net phase shift, $R = \langle r \rangle$ with r being the instantaneous bond length between absorber and backscatterer atoms, and $\sigma^{(n)}$ (n = 1, 2, 3, ...) are the cumulants describing Debye-Waller factors (DWFs).

Hence, the cumulants or DWFs are very important for the anharmonic XAFS where the even cumulants contribute to the amplitude, the odd ones to the phase of XAFS spectra, and for small anharmonicities, it is sufficient to keep the third and fourth cumulant terms [2]. They are crucial to quantitative treatment of XAFS spectra. Consequently, the lack of the precise DWFs or cumulants has been one of the biggest limitations to accurate structural determinations (e.g., the coordination numbers and the atomic distances) [3] and to specify the other properties of substances [4–8] from XAFS experiments. Therefore, investigation of DWFs or cumulants and XAFS is of great interest.

Many efforts have been made to overcome such limitations by the theoretical and experimental investigations, for example, see [1–26]. Unfortunately, there is still no simplified method which requires the calculations or measurements only for some leading quantities, yet provides all other theoretical and experimental XAFS values describing the thermodynamic properties, anharmonic effects and structural parameters of substances.

The purpose of this work is to study temperature dependence of the theoretical and experimental DWFs presented in terms of cumulant expansion up to the third order, thermal expansion coefficient, XAFS spectra and their Fourier transform magnitudes of Zn (hcp crystal) based on the method derived in this work using that the calculations and measurements are necessary only for the second cumulants or the mean square relative displacements (MSRDs) from which all other

* Corresponding author.
E-mail address: hungnv@vnu.edu.vn (N. Van Hung).

http://dx.doi.org/10.1016/j.physb.2017.06.027
Received 23 May 2017; Received in revised form 6 June 2017; Accepted 7 June 2017
Available online 08 June 2017
0921-4526/

theoretical and experimental XAFS parameters have been provided. This method has resulted (Section 2) based on the description of the quantum statistically derived analytical expressions for all the considered XAFS quantities in terms of second cumulants. The many-body effects included in the present one-dimensional model have been taken into account based on the first shell near neighbor contributions to the vibration between absorber and backscaterer atoms. Morse potential is assumed to describe the single-pair atomic interaction included in the anharmonic interatomic effective potential. Numerical results for Zn, an intensively used in science and technology, (Section 3) are found to be in good agreement with the experimental values measured at the Beamline BL8, Synchrotron Light Research Institute (SLRI, Thailand). They show evident temperature dependence of the thermodynamic properties, anharmonic effects and structural parameters of the considered material. The conclusions on the obtained results are presented in Section 4.

2. Theory

2.1. XAFS cumulants and thermal expansion coefficient of hcp crystals

In order to include anharmonic effects, the Hamiltonian of system in the present theory for hcp crystals (Zn) involves the anharmonic interatomic effective potential expanded up to the third order as

$$V_{eff}(x) \approx \frac{1}{2}k_{eff}x^2 + k_{3eff}x^3, \quad x = r - r_0, \tag{2}$$

where k_{eff} is the effective local force constant and k_{3eff} is the cubic anharmonic parameter giving an asymmetry of the anharmonic effective potential, r and r_0 are the instantaneous and equilibrium distances between absorber and backscatterer atoms, respectively.

The values of k_{eff} and k_{3eff} for hcp crystals included in all cumulants and XAFS expressions are determined based on the first shell near neighbors contributions approach (FNNCA) which was successfully applied to bcc crystals [8]. For hcp structure, each atom is bonded to 12 first shell near neighbors so that the anharmonic interatomic effective potential given by Eq. (2) contains not only the term describing the vibration between absorber and backscatterer atoms but also the other ones describing the projections of their pair-interactions with 22 first shell near neighbors along the bond direction except the absorber and backscatterer atoms themselves to take into account the many-body effects in the present theory.

The Morse potential expanded to the third order around its minimum

$$V(x) = D(e^{-2\alpha x} - 2e^{-\alpha x}) \approx D(-1 + \alpha^2x^2 - \alpha^3x^3), \tag{3}$$

is assumed to describe the single-pair atomic interaction included in the anharmonic effective potential where α describes the width of the potential and D is the dissociation energy.

For deriving XAFS cumulants we describe the anharmonic interatomic effective potential given by Eq. (2) in the summation of the harmonic contribution and a perturbation δV due to the weak anharmonicity as

$$V_{eff}(y) = \frac{1}{2}k_{eff}y^2 + \delta V(y), \quad \delta V \cong 5D\alpha^2ay + k_{3eff}y^3,$$
$$y = x - a, \quad a = < x > . \tag{4}$$

The derivation of XAFS cumulants for hcp crystals in this work is based on quantum statistical theory [27] and the parameters of the anharmonic interatomic effective potentials given by Eqs. (2) and (4), as well as an averaging procedure using the canonical partition function Z and statistical density matrix ρ, e.g.,

$$\langle y^m \rangle = \frac{1}{Z}Tr(\rho\, y^m), \quad m = 1, 2, 3, \cdots \tag{5}$$

Atomic vibrations are quantized in terms of phonons, and anharmonicity is the result of phonon-phonon interaction, that is why we express y in terms of the annihilation and creation operators, $\hat{a}$ and $\hat{a}^+$, respectively

$$y \equiv a_0(\hat{a} + \hat{a}^+), \quad a_0 = \sqrt{\frac{\hbar\omega_E}{10D\alpha^2}}, \tag{6}$$

which have the following properties

$$\hat{a}^+|n\rangle = \sqrt{n+1}\,|n+1\rangle, \ \hat{a}|n\rangle = \sqrt{n-1}\,|n-1\rangle,$$
$$[\hat{a}, \hat{a}^+] = 1, \ \hat{a}^+\hat{a}|n\rangle = n|n\rangle, \tag{7}$$

as well as use the harmonic oscillator state $|n\rangle$ as the eigenstate with the eigenvalue $E_n = n\hbar\omega_E$ for n being the phonon number, ignoring the zero-point energy for convenience.

Due to weak anharmonicity in XAFS, the canonical partition function in Eq. (5) can be expressed as

$$Z \cong Z_0 = \sum_n e^{-n\beta\hbar\omega_E} = \sum_{n=0}^{\infty} z^n = \frac{1}{1-z},$$
$$z = \exp(-\theta_E/T), \tag{8}$$

where the correlated Einstein frequency ω_E and temperature θ_E of hcp crystals are given by

$$\omega_E = \sqrt{\frac{10D\alpha^2}{M}}, \quad \theta_E = \frac{\hbar\omega_E}{k_B}, \tag{9}$$

M is the atomic mass and k_B is Boltzmann constant.

Using the above results for the correlated atomic vibration and the procedure depicted by Eqs. (5)–(9), as well as the first-order thermodynamic perturbation theory [27], the temperature-dependent XAFS cumulants have been derived.

Based on the procedure depicted by Eq. (5) we derived the even moment expressing the second cumulant or MSRD

$$\sigma^2(T) = \langle y^2 \rangle = \sum_n e^{-n\beta\hbar\omega_E}\langle n|y^2|n\rangle, \quad \beta = 1/k_BT, \tag{10}$$

and the odd moments expressing the first (m = 1) and third (m = 3) cumulants

$$\langle y^m \rangle = \frac{k_{eff}}{Z_0}\sum_{n,n'}\frac{e^{-\beta E_n} - e^{-\beta E_{n'}}}{E_n - E_{n'}}\langle n|\delta V(y)|n'\rangle\langle n'|y^m|n\rangle,$$
$$m = 1, 3, \tag{11}$$

where the operations expressed by Eqs. (5) and (6) have been applied to calculate the matrix elements given in Eqs. (10) and (11).

Consequently, the XAFS expressions have resulted for the second cumulant or MSRD

$$\sigma^2(T) = \langle y^2 \rangle = \sigma_0^2\frac{1+z(T)}{1-z(T)}, \quad \sigma_0^2 = \frac{\hbar\omega_E}{10D\alpha^2}, \tag{12}$$

for the first cumulant or net thermal expansion

$$\sigma^{(1)}(T) = a = \sigma_0^{(1)}\frac{1+z(T)}{1-z(T)} = \frac{\sigma_0^{(1)}}{\sigma_0^2}\sigma^2(T),$$
$$\sigma_0^{(1)} = \frac{3\alpha}{4}\sigma_0^2, \tag{13}$$

and for the third cumulant or mean cubic relative displacement (MCRD)

$$\sigma^{(3)}(T) = \langle y^3 \rangle = \sigma_0^{(3)}\left[3\left(\frac{\sigma^2(T)}{\sigma_0^2}\right)^2 - 2\right],$$
$$\sigma_0^{(3)} = \frac{\alpha}{2}(\sigma_0^2)^2. \tag{14}$$

Moreover, using the first cumulant given by Eq. (13), the expression for the thermal expansion coefficient has been derived and given by

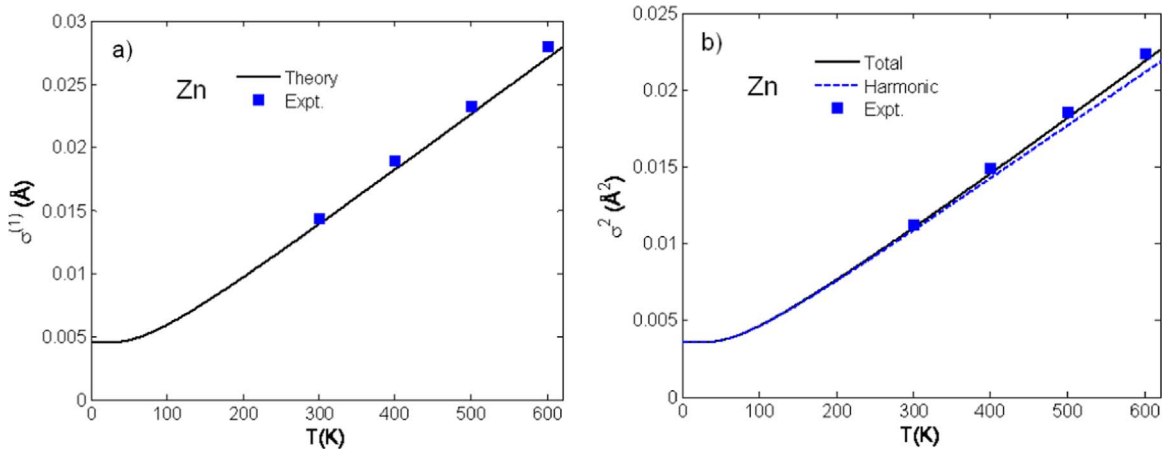

Fig. 1. Temperature dependence of (a) first cumulant $\sigma^{(1)}$(T) and (b) total and harmonic second cumulants $\sigma^2_{tot}(T)$ and σ^2(T), respectively, of Zn calculated using the present theory compared to the experimental values at 300 K, 400 K, 500 K and 600 K.

$$\alpha_T(T) = \frac{1}{r}\frac{da}{dT} = \alpha_T^0\frac{(\sigma^2(T))^2 - (\sigma_0^2)^2}{T^2},$$
$$\alpha_T^0 = \frac{15D\alpha^3}{4k_B r}. \quad (15)$$

In the above obtained expressions, $\sigma_0^{(1)}$, σ_0^2, $\sigma_0^{(3)}$ are zero-point energy contributions to three first XAFS cumulants $\sigma^{(1)}$(T), σ^2(T), $\sigma^{(3)}$(T), respectively, and α_T^0 is the constant value which the thermal expansion coefficient approaches at high-temperatures.

Note that the second cumulant given by Eq. (12) is harmonic while the experimental data always include the temperature-dependent anharmonic effects. That is why we introduce the total second cumulant or MSRD as

$$\sigma^2_{tot}(T) = \sigma^2(T) + \sigma^2_A(T), \quad (16)$$

which involves an anharmonic contribution

$$\sigma^2_A(T) = \beta_A(T)[\sigma^2(T) - \sigma_0^2], \quad (17)$$

containing the anharmonic factor

$$\beta_A(T) = \frac{9\alpha^2}{8}\sigma^2(T)\left[1 + \frac{3\alpha}{4R}\sigma^2(T)\left(1 + \frac{3\alpha}{4R}\sigma^2(T)\right)\right], \quad (18)$$

derived based on the relative volume change due to thermal expansion and described also in terms of second cumulant.

Hence, the above derived expressions for the first, second cumulants and thermal expansion coefficient $\sigma^{(1)}$, $\sigma^{(3)}$ and α_T, respectively, are described in terms of second cumulant σ^2 or MSRD. Moreover, the total second cumulant given by Eqs. (16)–(18) including anharmonic effects is presented also in terms of second cumulant. This description is useful to create the present method based on that the calculations and measurements are necessary only for the second cumulants from which the first, third cumulants, thermal expansion coefficient and other XAFS parameters can be provided.

2.2. Anharmonic XAFS based on cumulant expansion

Further, we develop the XAFS function given by Eq. (1) into an analytical form explicitly including the above obtained cumulants for the temperature-dependent K-edge anharmonic XAFS spectra as

$$\chi(k, T) = \sum_j \frac{S_0^2 N_j}{kR_j^2}F_j(k)F_A(k, T)e^{-(2k^2\sigma^2(T)+2R_j/\lambda(k))}$$
$$\sin(2kR_j + \Phi_j(k) + \Phi_A^j(k, T)), \quad (19)$$

which contains the anharmonic contribution to amplitude described by an factor

$$F_A(k, T) = \exp[-2k^2\sigma_A^2(T)], \quad (20)$$

causing the anharmonic attenuation and the anharmonic contribution to phase

$$\Phi_A(T, k) = 2k\left[\sigma^{(1)}(T) - 2\sigma_A^2(T)\left(\frac{1}{R} - \frac{1}{\lambda(k)}\right) - \frac{2}{3}\sigma^{(3)}(T)k^2\right], \quad (21)$$

causing the anharmonic phase shift of XAFS spectra.

In the anharmonic XAFS function Eq. (19) S_0^2 is the square of the many body overlap term, N_j is the atomic number of each shell, the second cumulant σ^2 and its anharmonic contribution σ_A^2 are calculated by Eqs. (12) and (17), respectively, the mean free path λ is defined by the imaginary part of the complex photoelectron momentum $p = k + i/\lambda$, and the sum is over all considered atomic shells. Moreover, all parameters of this function can be obtained from the second cumulant or MSRD, and this function will return to the harmonic case calculated by the well-known FEFF code [28] if the anharmonic contributions to amplitude F_A(k,T) and to phase Φ_A(k,T) are excluded. Inversely, the FEFF code can also be modified by including these anharmonic contributions to XAFS amplitude and phase to calculate the anharmonic XAFS spectra and their Fourier transform magnitudes. It is the evident advantage of the present method which will be applied to the numerical calculations and to the extractions of experimental XAFS parameters for Zn presented in Section 3.

3. Experimental and numerical results and discussions

3.1. Experimental

The measurements of the second cumulant, XAFS spectra and their Fourier transform magnitudes of Zn at 300 K, 400 K, 500 K and 600 K have been performed at the Beamline BL8, SLRI (Thailand). It is the routinely operated for X-ray absorption spectroscopy (XAS) in an immediate photon energy range (1.25–10 keV). The experimental set-up conveniently facilitates XAS measurements in transmission and fluorescence-yield modes at several K-edges of elements ranging from Magnesium to Zinc [29]. The experimental values of the first, third cumulants, thermal expansion coefficients and some other XAFS parameters of Zn at 300 K, 400 K, 500 K and 600 K have been extracted from the measured values of the second cumulant using the present method based on the description of these quantities in terms of second cumulant presented in Section 2.1. The obtained experimental results will be presented in Section 3.2 compared to the theoretical results.

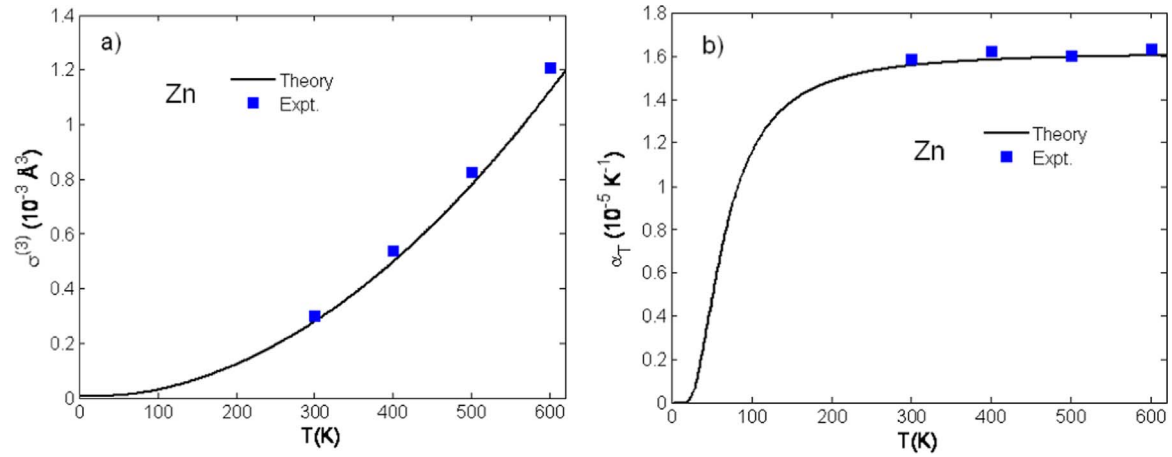

Fig. 2. Temperature dependence of (a) third cumulant $\sigma^{(3)}$(T) and (b) thermal expansion coefficient α_T(T) of Zn calculated using the present theory compared to the experimental values at 300 K, 400 K, 500 K and 600 K.

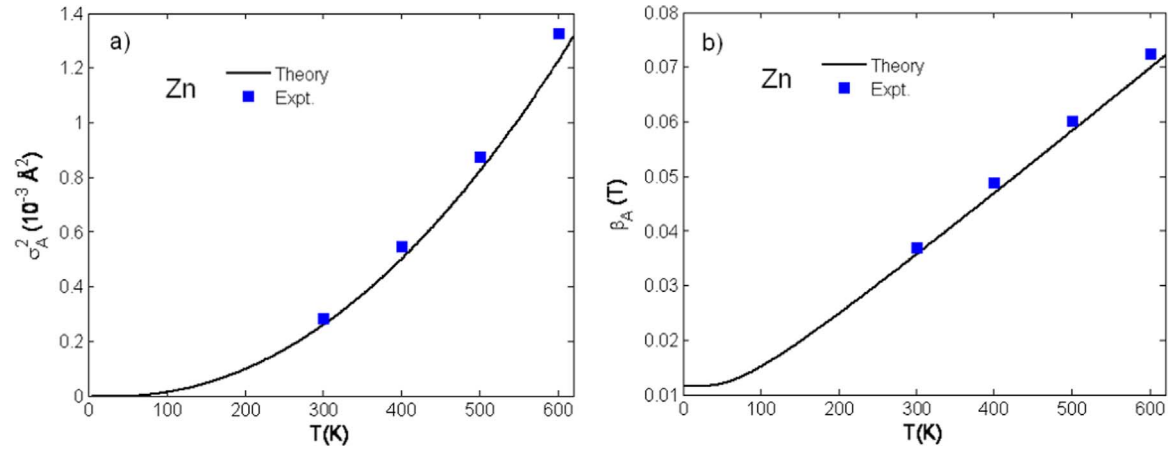

Fig. 3. Temperature dependence of (a) anharmonic contribution $\sigma_A^2(T)$ to second cumulant or MSRD and (b) anharmonic factor β_A(T) of Zn calculated using the present theory compared to the experimental values at 300 K, 400 K, 500 K and 600 K.

3.2. Numerical calculation results compared to experiment and discussions

Now the expressions derived in the previous Section 2 are applied to numerical calculations for Zn using its Morse potential parameters [30] D = 0.1700 eV, α = 1.7054 Å^{-1} which were obtained using experimental values for the energy of sublimation, the compressibility, and the lattice constant.

3.2.1. XAFS cumulants and thermal expansion coefficient

Fig. 1 illustrates good agreement of (a) first cumulant $\sigma^{(1)}$(T) and (b) total and harmonic second cumulants $\sigma_{tot}^2(T)$, σ^2(T), respectively, of Zn calculated using the present theory with the experimental values at 300 K, 400 K, 500 K, and 600 K. Here, $\sigma_{tot}^2(T)$ is a little different from σ^2(T) at temperatures greater than the room temperature due to the temperature-dependent anharmonic contributions. Note that using this first cumulant we can obtain temperature dependence of the first shell near neighbor distance based on the expression R(T) = R(0) + $\sigma^{(1)}$(T).

Temperature dependence of third cumulant $\sigma^{(3)}$(T) (Fig. 2a) and thermal expansion coefficient α_T(T) (Fig. 2b) of Zn calculated using the present theory agrees well with the experimental values at 300 K, 400 K, 500 K and 600 K. Here, the theoretical and experimental thermal expansion coefficients of Zn approach the constant values at high-temperatures as it was obtained for the other crystal structures [11,22–26].

Fig. 3 illustrate good agreement of temperature dependence of (a) anharmonic contributions $\sigma_A^2(T)$ to the second cumulant or MSRD and (b) anharmonic factor β_A(T) of Zn calculated using the present theory with their experimental values at 300 K, 400 K, 500 K and 600 K where β_A(T) characterizes percentage of the anharmonic contributions at each temperature. These values are normally difficult to be directly measured, but using the present method they have been calculated and extracted from the calculated and measured second cumulants.

The cumulant ratios $\sigma^{(1)}\sigma^2/\sigma^{(3)}$ and $\alpha_T T\sigma^2/\sigma^{(3)}$ are often considered as the standards for cumulant studies [6–9,22,25,26] and to identify the temperature above which the classical limit is applicable [22]. Fig. 4 show good agreement of temperature dependence of (a) $\sigma^{(1)}\sigma^2/\sigma^{(3)}$ and (b) $\alpha_T T\sigma^2/\sigma^{(3)}$ of Zn calculated using the present theory with the experimental values at 300 K, 400 K, 500 K and 600 K. The theoretical and experimental results of these ratios show that above the Einstein temperature (θ_E = 206 K calculated using the present theory for Zn) they approach the classical value [7,9] of 1/2 so that the classical limit is applicable.

Table 1 illustrates good agreement of the values of three first XAFS cumulants and thermal expansion coefficients of Zn calculated using the present theory at 300 K, 400 K, 500 K and 600 K with their experimental values.

The second cumulant describing MSRD is primary a harmonic effect plus small anharmonic contributions which appear only at high-temperatures. But the first cumulant describing the net thermal expansion or lattice disorder, the third cumulant or MCRD describing the asymmetry of pair atomic distribution function and the thermal expansion coefficient are

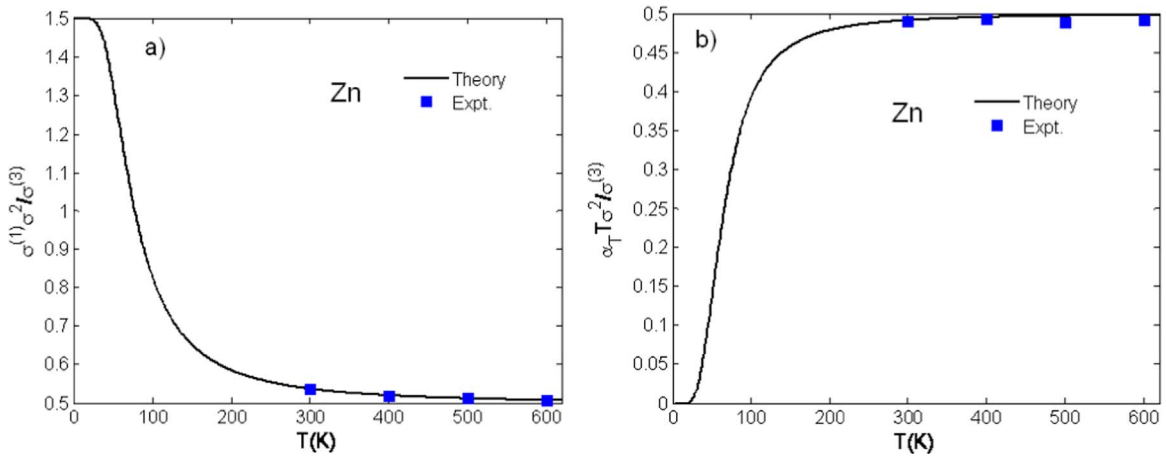

Fig. 4. Temperature dependence of cumulant ratios (a) $\sigma^{(1)}\sigma^2/\sigma^{(3)}$ and (b) $\alpha_T T\sigma^2/\sigma^{(3)}$ of Zn calculated using the present theory compared to the experimental values at 300 K, 400 K, 500 K and 600 K.

Table 1
Comparison of the values of three first XAFS cumulants and thermal expansion coefficients of Zn calculated using the present theory with their experimental values at 300 K, 400 K, 500 K and 600 K.

T(K)	$\sigma^{(1)}$ (Å) Theory	$\sigma^{(1)}$ (Å) Expt.	σ^2 (Å^2) Total	σ^2 (Å^2) Harm.	σ^2 (Å^2) Expt.	$\sigma^{(3)}$ (Å^3) Theory	$\sigma^{(3)}$ (Å^3) Expt.	α_T (10^{-5}/K) Theory	α_T (10^{-5}/K) Expt.
300	0.0139	0.0143	0.0110	0.0109	0.0113	0.0003	0.0003	1.555	1.582
400	0.0182	0.0189	0.0146	0.0143	0.0149	0.0005	0.0006	1.582	1.618
500	0.0226	0.0232	0.0182	0.0177	0.0185	0.0008	0.0009	1.595	1.599
600	0.0270	0.0279	0.0219	0.0211	0.0223	0.0011	0.0012	1.602	1.630

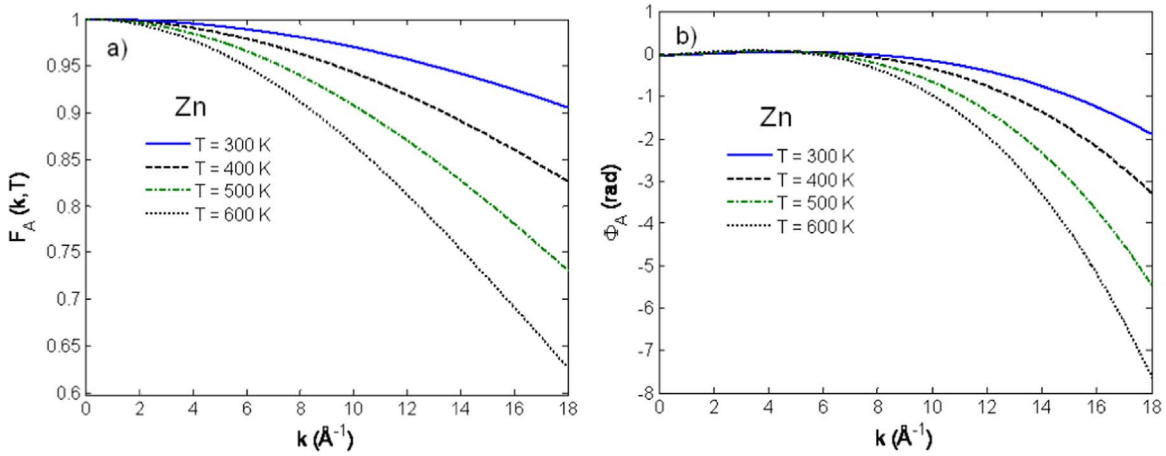

Fig. 5. The wave number k-dependence of the anharmonic (a) attenuation factor $F_A(k,T)$ and (b) phase shift $\Phi_A(k,T)$ of XAFS of Zn at 300 K, 400 K, 500 K, and 600 K calculated using the present theory.

entirely anharmonic effects because they appear due to including the cubic anharmonic effective potential parameter.

3.2.2. XAFS spectra and their Fourier transform magnitudes

Based on the present derived method, the FEFF code [28] has been modified by including the amharmonic contributions to XAFS amplitude and phase described by the above obtained cumulants to calculate XAFS spectra at 300 K, 400 K, 500 K, 600 K of Zn and their Fourier transform magnitudes. Fig. 5 illustrate the anharmonic (a) attenuation factor $F_A(k,T)$ and (b) phase shift $\Phi_A(k,T)$ of XAFS of Zn at 300 K, 400 K, 500 K, and 600 K calculated using the present theory including the above obtained cumulants. These values increase showing the increase of anharmonicity as k-value and temperature T increase. Using these values of $F_A(k,T)$ and $\Phi_A(k,T)$, the anharmonic XAFS spectra of Zn at 300 K, 400 K, 500 K and 600 K have been calculated and presented in Fig. 6a compared to the measured results presented in Fig. 6b. The anharmonic amplitude attenuation and phase shift are evidently shown in both theoretical and experimental XAFS spectra. These theoretical and experimental anharmonic XAFS spectra have been Fourier transformed and their Fourier transform magnitudes are presented in Fig. 7. They show good agreement between the theoretical and experimental results, as well as the decrease of the peak heights and their shifts to the left as the temperature T increases.

Note that the anharmonic XAFS spectra of Zn at 300 K, 400 K, 500 K and 600 K and their Fourier transform magnitudes have been calculated based on including the anharmonic contributions to XAFS amplitude and phase using the cumulants obtained from the second cumulants or MSRDs. The results are found to be in good agreement with the measured data. Moreover, using the present theory and the measured second cumulants of Zn at 300 K, 400 K, 500 K, 600 K we have reproduced all the considered experimental values including XAFS spectra and their Fourier transform magnitudes. The obtained results agree well with the experimental values at these temperatures.

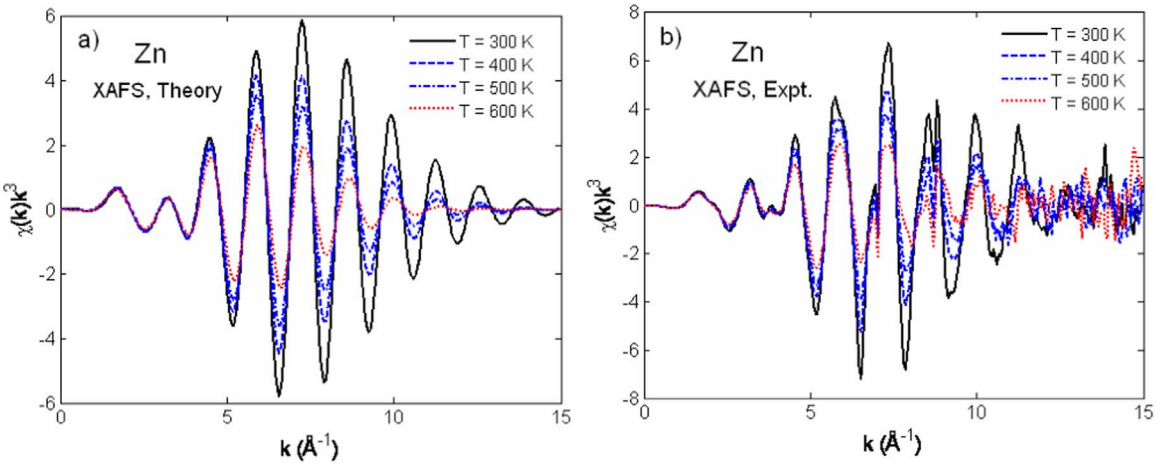

Fig. 6. (a) Theoretical and (b) experimental XAFS spectra of Zn at 300 K, 400 K, 500 K, 600 K.

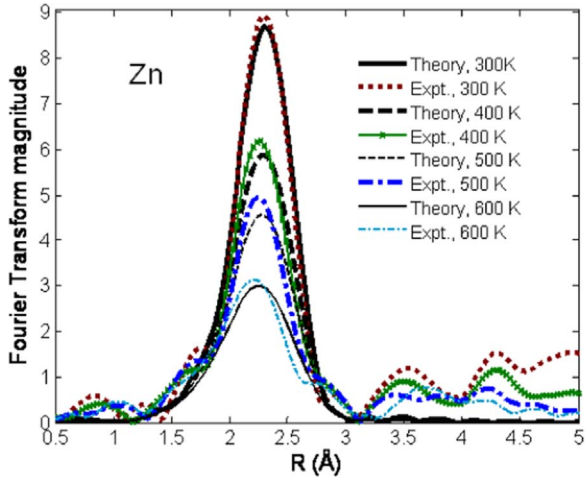

Fig. 7. Comparison of Fourier transform magnitudes of XAFS spectra of Zn at 300 K, 400 K, 500 K, and 600 K calculated using the present theory with their experimental results.

4. Conclusions

In this work, temperature dependence of the theoretical and experimental DWFs presented in terms of cumulant expansion up to the third order, thermal expansion coefficient, XAFS spectra and their Fourier transform magnitudes of Zn has been studied. The obtained quantities contribute to the valuation of the thermodynamic properties of Zn, as well as to including the anharmonic effects in XAFS and their Fourier transform magnitudes providing the accurate structural determination of the considered crystal. This method has been successfully used for Zn and it can also be applied to studying XAFS quantities of other hcp crystals.

The most advantageous development in this work is the quantum statistically derived method based on which all the considered theoretical and experimental XAFS quantities including those which are difficult to be directly measured have been obtained and extracted from the calculated and measured second cumulant or MSRD. Therefore, it has significantly simplified and reduced the XAFS calculations and measurements, yet provides all necessary theoretical and experimental XAFS data.

The obtained temperature-dependent theoretical and experimental XAFS quantities have been in detail analyzed and valuated. They include the evident anharmonic effects and satisfy all their fundamental properties, as well as approach the classical values at high-temperatures and contain zero-point energy contributions at low-temperatures, a quantum effect.

The good agreement between the theoretical and experimental XAFS quantities of Zn, as well as their good description of temperature dependence of the thermodynamic properties and anharmonic effects in XAFS of Zn, illustrate the simplicity and efficiency of the present method in XAFS data analysis and in materials studies.

Acknowledgements

The authors thank Prof. J.J. Rehr and Prof. Paolo Fornasini for useful comments. One of the authors (CST) thanks Dr. Wantana Klysubun, the head of Beamline BL8, and the Synchrotron Light Research Institute (Thailand) for hospitality and assistance during his stay their to perform the necessary measurements. This research is funded by the Vietnam National Foundation for Science and Technology Development (NAFOSTED) under Grant no. 103.01-2015.10.

References

[1] E.D. Crozier, J.J. Rehr, R. Ingalls, D.C. Koningsberger, R. Prins (Eds.), X-ray Absorption, Wiley, New York, 1988 (Chap. 9).
[2] J.M. Tranquada, R. Ingalls, Phys. Rev. B 28 (1983) 3520.
[3] F.D. Vila, J.J. Rehr, H.H. Rossner, H.J. Krappe, Phys. Rev. B 76 (2007) 014301.
[4] N.V. Hung, V.V. Hung, H.K. Hieu, R.R. Frahm, Phys. B 406 (2011) 456.
[5] N.V. Hung, C.S. Thang, N.C. Toan, H.K. Hieu, VAC 101 (2014) 63.
[6] N.V. Hung, J. Phys. Soc. Jpn. 83 (2014) 024802.
[7] N.V. Hung, T.S. Tien, N.B. Duc, D.Q. Vuong, Mod. Phys. Lett. B 28 (2014) 1450174.
[8] N.V. Hung, T.T. Hue, H.D. Khoa, D.Q. Vuong, Phys. B 503 (2016) 174.
[9] E.A. Stern, P. Livins, Zhe Zhang, Phys. Rev. B 43 (1991) 8850.
[10] L. Tröger, T. Yokoyama, D. Arvanitis, T. Lederer, M. Tischer, K. Baberschke, Phys. Rev. B 49 (1994) 888.
[11] A.I. Frenkel, J.J. Rehr, Phys. Rev. B 48 (1993) 585.
[12] T. Miyanaga, T. Fujikawa, J. Phys. Soc. Jpn. 63 (1994) (1036 and 3683).
[13] T. Yokoyama, Phys. Rev. B 57 (1998) 3423.
[14] A.V. Poiarkova, J.J. Rehr, Phys. Rev. B 59 (1999) 948.
[15] G. Dalba, P. Fornasini, R. Grisenti, J. Purans, Phys. Rev. Lett. 82 (1999) 4240.
[16] I.V. Pirog, T.I. Nedoseikina, Phys. B 334 (2003) 123.
[17] J.J. Rehr, J.J. Kas, M.P. Prange, A.P. Sorini, Y. Takimoto, F. Villa, C. R. Phys. 10 (2009) 548.
[18] P. Fornasini, R. Grisenti, J. Synchrotron Radiat. 22 (2015) 1242.
[19] N.V. Hung, R. Frahm, Physica B 208 & 209 (1995) 91.
[20] N.V. Hung, R. Frahm, H. Kamitsubo, J. Phys. Soc. Jpn. 65 (1996) 3571.
[21] N.V. Hung, J. Phys. IV Fr. 7 (1997) C2–279.
[22] N.V. Hung, J.J. Rehr, Phys. Rev. B 56 (1997) 43.
[23] N.V. Hung, N.B. Duc, R.R. Frahm, J. Phys. Soc. Jpn. 72 (2003) 1254.
[24] M. Daniel, D.M. Pease, N. Van Hung, J.I. Budnick, Phys. Rev. B 69 (2004) 134414.
[25] N.V. Hung, P. Fornasini, J. Phys. Soc. Jpn. 76 (2007) 084601.
[26] N.V. Hung, N.B. Trung, B. Kirchner, Physica B 405 (2010) 2519.
[27] R.P. Feynman, Statistical Mechanics, Benjamin, Reading, 1972.
[28] J.J. Rehr, J. Mustre de Leon, S.I. Zabinsky, R.C. Albers, J. Am. Chem. Soc. 113 (1991) 5135.
[29] W. Klysubun, P. Sombunchoo, W. Deenam, C. Komark, J. Synchrotron Radiat. 19 (2012) 930.
[30] N.V. Hung, Commun. Phys. (CIP) 14 (1) (2004) 7–14.